Research Article **Open Access**

Marek Macák*, Róbert Čunderlík, Karol Mikula, and Zuzana Minarechová

An upwind-based scheme for solving the oblique derivative boundary-value problem related to physical geodesy

DOI 10.1515/jogs-2015-0018
Received May 19, 2015; accepted December 10, 2015

Abstract: The paper presents a novel original upwind-based approach for solving the oblique derivative boundary value problem by the finite volume method. In this approach, the oblique derivative boundary condition is interpreted as a stationary advection equation for the unknown disturbing potential. Its approximation is then performed by using the first order upwind scheme taking into account information from inflow parts of the finite volume boundary only. When the numerical scheme is derived, numerical simulations in 2D and 3D domains are performed and the experimental order of convergence of the proposed algorithm is studied. Moreover a comparison with a solution by the central scheme previously used for this kind of problem is performed. Finally we present numerical experiments dealing with the global and local gravity field modelling.

Keywords: Finite volume method, Oblique derivative boundary-value problem, Upwind principle

1 Introduction

A determination of the Earth's gravity field is usually formulated in terms of the geodetic boundary-value problem (BVP). At present, terrestrial gravimetric measurements are often accompanied by the precise GNSS positioning. Such a combination yields gravity disturbances that naturally lead to boundary conditions (BC) for the fixed gravimetric BVP (FGBVP). From the mathematical point of view, FGBVP represents an exterior oblique derivative BVP for the Laplace equation, cf. (Koch and Pope 1972; Bjerhammar and Svensson 1983; Holota 1997). In the last decades several researchers have been dealing with such kind of BVP, e.g. (Freeden and Kersten 1981; Bauer 2004; Gutting 2007, 2012; Čunderlík et al. 2008, 2012; Grothaus and Raskop 2009). In this paper we present an upwind-based approach for solving the oblique derivative BVP that is based on the finite volume method (FVM).

Nowadays, efficient numerical methods like the finite element method (FEM), boundary element method (BEM) or FVM are often used to solve various engineering problems. In physical geodesy they still represent alternatives to classical approaches (e.g. the spherical harmonic (SH) analysis, radial basis functions, least squares collocation or integral transforms) that are usually preferred for gravity field modelling. Nevertheless, obvious advantages of the numerical methods like a straightforward refinement of the discretization, opportunity to consider real topography or feasibility for high-resolution modelling make these methods perspective for further investigation.

The first application of FEM to gravity field modelling has been introduced by Meissl (1981), later studied in (Shaofeng and Dingbo 1991) and (Fašková et al. 2010). In case of BEM, two approaches have been developed. The first one has been based on the indirect BEM formulation and the Galerkin BEM (Klees 1995, 1998; Lehmann 1997; Lehmann and Klees 1999; Klees et al. 2001) and the second one on the direct BEM formulation and the collocation technique (Čunderlík et al. 2008; Čunderlík and Mikula 2010). The variational method based on a weak formulation and a functional minimization has been studied in (Holota and Nesvadba 2008). In case of FVM, the basic numerical scheme for BVP with the Neumann BC has been introduced by Fašková (2008) and its parallel implementation by Minarechová et al. (2015).

The first insight of FVM applied to the oblique derivative BVP has been discussed in (Macák et al. 2012). Later on, a central numerical scheme for the oblique derivative

***Corresponding Author: Marek Macák:** Department of Mathematics and Descriptive Geometry, Faculty of Civil Engineering, Slovak University of Technology, Radlinského 11, 810 05 Bratislava, Slovakia, E-mail: macak@math.sk
Róbert Čunderlık, Karol Mikula, Zuzana Minarechová: Department of Mathematics and Descriptive Geometry, Faculty of Civil Engineering, Slovak University of Technology, Radlinského 11, 810 05 Bratislava, Slovakia

BVP has been developed and efficiently applied to gravity field modelling (Macák et al. 2014). From the mathematical point of view it is known that this central numerical scheme can lead to nonphysical oscillations.

The objective of this paper is to introduce a new upwind-based numerical scheme in which the oblique derivative boundary condition is interpreted as a stationary advection equation for the unknown disturbing potential. Such an approach is more robust and avoids the oscillations. The numerical simulations aim to demonstrate this advantage while comparing both schemes. Finally the proposed upwind numerical scheme is applied to global and local gravity field modelling.

2 Formulation of the oblique derivative BVP

Let us consider the fixed gravimetric BVP, cf. (Koch and Pope, 1972; Bjerhammar and Svensson, 1983; Holota, 1997):

$$\Delta T(\mathbf{x}) = 0, \mathbf{x} \in R^3 - S, \tag{1}$$

$$\nabla T(\mathbf{x}) \cdot \vec{s}(\mathbf{x}) = \delta g(\mathbf{x}), \mathbf{x} \in \partial S, \tag{2}$$

$$T(\mathbf{x}) \to 0, \quad \text{as} \quad |\mathbf{x}| \to \infty, \tag{3}$$

where S is the Earth, $T(\mathbf{x})$ is the disturbing potential defined as a difference between the real and normal gravity potential at any point $\mathbf{x} = (x, y, z)$, $\delta g(\mathbf{x})$ is the so-called gravity disturbance and $\vec{s}(\mathbf{x}) = \nabla U(\mathbf{x})/|\nabla U(\mathbf{x})|$ is the unit vector normal to the equipotential surface of the normal potential $U(\mathbf{x})$ at any point $\mathbf{x}$.

The satellite missions like the Challenging Minisatellite Payload (CHAMP) (Reigber et al., 2002), the Gravity Recovery And Climate Experiment (GRACE) (Tapley, 2004) and the Gravity Field and Steady-State Ocean Circulation Explorer (GOCE) (ESA, 1999) have brought a significant improvement in determination of the low-frequency part of the gravity field. Since in our approach we are solving BVP in a spatial domain, the information obtained from these satellite missions is incorporated in our solution in the form of the Dirichlet BC prescribed on an additional upper boundary (Fig.1a). Altitude of this boundary is chosen to approximate the orbit of the GOCE satellite mission. Hence, in the following we consider the bounded domain Ω (Fig. 1) where we solve the modified FGBVP in the form, c.f. (Fašková et al. 2010) or (Minarechová et al. 2015):

$$\Delta T(\mathbf{x}) = 0, \mathbf{x} \in \Omega, \tag{4}$$

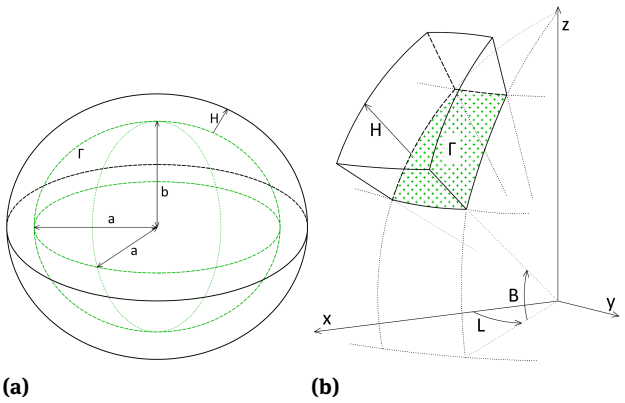

Figure 1: The computational domain Ω for a) global numerical experiment, b) local numerical experiment. The dotted boundary Γ represents the part of the Earth's surface. B, L and H denote ellipsoidal latitude, longitude and height, respectively.

$$\nabla T(\mathbf{x}) \cdot \vec{s}(\mathbf{x}) = \delta g(\mathbf{x}), \mathbf{x} \in \Gamma, \tag{5}$$

$$T(\mathbf{x}) = T_{SAT}(\mathbf{x}), \mathbf{x} \in \partial\Omega - \Gamma, \tag{6}$$

where T_{SAT} represents the disturbing potential generated from a chosen SH-based satellite-only geopotential model. The bottom boundary Γ represents the Earth's surface. It is worth to noting that we are looking for a solution in the bounded domain Ω, so we do not deal with a regularity of this solution at infinity. In the caseof local gravity field modelling, four additional side boundaries are considered (Fig. 1b). Here the Dirichlet BC in the form of the disturbing potential generated from a satellite-only geopotential model can be prescribed as well. An impact of such BC on the obtained numerical solution has been studied by Fašková et al. (2010). The mathematical theory for a solution of the Laplace equation (4) with mixed BCs (5)-(6) has been discussed in (Lieberman, 2013).

3 Solution to the oblique derivative BVP by the finite volume method

To solve the modified FGBVP (4)-(6), the FVM has been chosen. The general approach by the FVM, see (Eymard et al., 2001), is to divide the computational domain Ω into finite volumes p and integrate the Laplace equation over each finite volume with a use of the divergence theorem that turns the volume integrals into surface integrals.

Let us denote $q \in N(p)$ as a neighbour of the finite volume p and $N(p)$ denotes all neighbours of p. Let T_p and T_q be approximate values of T in p and q, e_{pq} be a boundary

of the finite volume p common with q, $m(e_{pq})$ is the area of e_{pq}. Let $\mathbf{x}_p$ and $\mathbf{x}_q$ be representative points of p and q respectively and d_{pq} their distance. If we approximate the normal derivative along the boundary of the finite volume p by differences between T_p and T_q divided by d_{pq} we obtain the following equation for every finite volume p

$$\sum_{q\in N_p} \frac{m(e_{pq})}{d_{pq}}(T_p - T_q) = 0, \tag{7}$$

which forms together the linear system of algebraic equations. The term $\frac{m(e_{pq})}{d_{pq}}$ defined on sides of the finite volume $p$is the so-called transmissivity coefficient, see (Eymard et al., 2001). To take BCs into account, in case of the Dirichlet BC (6) we prescribe the value of T_q on the boundary, while in case of the oblique derivative BC (5), a special treatment is needed. In Macák et al. (2014) we have introduced a central numerical scheme to approximate the oblique derivative BC. Since such an approach can lead to nonphysical oscillations, here we present an upwind-based scheme that will be discussed in the following subsection.

3.1 The upwind scheme for solving oblique derivative BVP

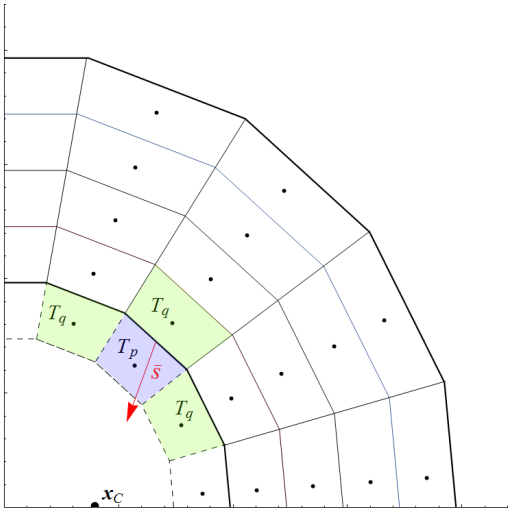

Figure 2: Illustration of the 2D FVM grid. The dashed lines denote the boundaries of added finite volumes, the volume of interest tis shown in blue and its neighboring volumes in green. The vectors $\vec{s}$ are depicted by red.

One can rewrite the divergence of $T(\mathbf{x})\vec{s}(\mathbf{x})$ in the form

$$\nabla\cdot(T(\mathbf{x})\vec{s}(\mathbf{x})) = T(\mathbf{x})\nabla\cdot\vec{s}(\mathbf{x}) + \nabla T(\mathbf{x})\cdot\vec{s}(\mathbf{x}). \tag{8}$$

By inserting (5) into Eq. (8), we obtain

$$\nabla\cdot(T(\mathbf{x})\vec{s}(\mathbf{x})) - T(\mathbf{x})\nabla\cdot\vec{s}(\mathbf{x}) = \delta g(\mathbf{x}). \tag{9}$$

We add one row of finite volumes under the bottom boundary, see Fig. 2, and integrate (9) over one of the added finite volumes p (we omit $(\mathbf{x})$ to simplify the notation in the following equations)

$$\int_p \nabla\cdot(T\vec{s})dV - \int_p T\nabla\cdot\vec{s}dV = \int_p \delta g dv, \tag{10}$$

where dV is the volume element. Using a constant approximation of the solution T on the finite volume p denoted by T_p and applying the divergence theorem to the left-hand side of the Eq. (10) we obtain

$$\sum_{q\in N(p)}\int_{e_{pq}} T\vec{s}\cdot\vec{n}_{pq}dS - \sum_{q\in N(p)} T_p\int_{e_{pq}}\vec{s}\cdot\vec{n}_{pq}dS = \int_p \delta g dV, \tag{11}$$

where dS is the surface area element and $\vec{n}_{pq}$ is a unit normal vector oriented from p to q. Denoting a constant approximation of the solution on the interface e_{pq} by T_{pq} and a volume of the finite volume p by $m(p)$ yields

$$\sum_{q\in N(p)} T_{pq}\int_{e_{pq}}\vec{s}\cdot\vec{n}_{pq}dS - \sum_{q\in N(p)} T_p\int_{e_{pq}}\vec{s}\cdot\vec{n}_{pq}dS = \delta g m(p). \tag{12}$$

When we denote

$$s_{pq} = \int_{e_{pq}}\vec{s}\cdot\vec{n}_{pq}dS \approx m(e_{pq})\vec{s}\cdot\vec{n}_{pq}, \tag{13}$$

we finally obtain

$$\sum_{q\in N(p)} s_{pq}(T_{pq} - T_p) = \delta g m(p). \tag{14}$$

Due to an analogy of the oblique derivative BC (2) and the stationary advection equation we applied an upwind principle, which is used exclusively in solving advection equations in fluid dynamics (LeVeque, 2002). Then we define

$$T_{pq} = T_p, \quad \text{if} \quad s_{pq} > 0, \tag{15}$$

$$T_{pq} = T_q, \quad \text{if} \quad s_{pq} < 0, \tag{16}$$

which correspond to the inflow part to the finite volume $p(s_{pq} <0)$ and outflow part to the finite volume $p(s_{pq} >0)$ when $\vec{s}$ is understood as an advection velocity vector. By using (15)-(16) in (14) we obtain the final form of an approximation to the oblique derivative BC (5) as

$$\sum_{q\in N(p)^{in}} s_{pq}(T_q - T_p) = \delta g m(p), \tag{17}$$

where $N(p)^{in}$ is a set of neighbours at the inflow boundaries of the finite volume p, i.e. where s_{pq}<0.

Using (17), we get the right-hand side vector with nonzero entries and modified diagonal coefficients for finite volumes along the boundary. Hence, the system matrix is nonsymmetric and diagonally dominant.

4 Numerical experiments

In this section, we present several numerical experiments which were performed in order to test the proposed upwind scheme. The numerical scheme will be qualified according to the value of the so-called experimental order of convergence (EOC) that can be computed as follows. If we assume that the error of the scheme in some norm is proportional to some power of the grid size, i.e., $Error(h) = Ch^{\epsilon}$, with a constant C, then having two grids with sizes h_1 and h_2, where $h_1 > h_2$, yields two errors $Error(h_1) = C(h_1)^{\epsilon}$ and $Error(h_2) = C(h_2)^{\epsilon}$ from where we can simply extract $\epsilon = \log_{\frac{h_1}{h_2}}(Error(h_1)/Error(h_2))$. If $h_2 = \frac{h_1}{2}$ then $\epsilon = \log_2(Error(h_1)/Error(h_2))$.

Then the ϵ is the EOC and can be determined by comparing numerical solutions and exact solutions on subsequently refined grids.

In numerical experiments, we present statistical characteristics of residuals, namely:

- the mean value $\overline{res} = \frac{1}{n}\sum_{p=1}^{n} res_p$, where $n = n_1 n_2$, or $n = n_1 n_2 n_3$
- the standard deviation $(STD) = \sqrt{\frac{1}{n}\sum_{p=1}^{n}(res_p - \overline{res})^2}$,
- the MAX-norm on bottom boundary $\Gamma(MAX(\Gamma)) = \max_{p\in\Gamma}|res|$
- the L2-norm in domain Ω $(L_2(\Omega)) = \sqrt{\sum_{p=1}^{n}(res_p)^2 m(p)}$,

where res_p=$T_p - T_p^{\star}$, where $T_p^{\star}$ is either exact or EGM2008 value in a representative point of the finite volume p, n_1, n_2 and n_3 are the numbers of divisions in L, B, H directions.

4.1 Numerical simulations

First, let us consider the oblique derivative BC defined by Eq. (2). The gravity disturbance as a difference between magnitudes of the real and normal gravity represents a projection of $\nabla T(\mathbf{x})$ into the unit vector $\vec{s}(\mathbf{x})$. The oblique derivative arises from the fact that the direction of $\vec{s}(\mathbf{x})$ in general does not coincide with the normal $\vec{n}(\mathbf{x})$ to the Earth's surface. It means that here we can distinguish two angles; the first one between $\vec{n}(\mathbf{x})$ a $\vec{s}(\mathbf{x})$ is known, while the second one between $\nabla T(\mathbf{x})$ and $\vec{s}(\mathbf{x})$ is unknown due to an unknown direction of $\nabla T(\mathbf{x})$. To simulate uch a situation in our upwind scheme we perform the following testing experiments.

In the first experiment, we have considered the annulus between two circles with radii $R_d = 1$ m and $R_u = 2$ m. As the Dirichlet BC (6) on the upper boundary, the chosen exact solution of (4) in the form $T^{\star} = -\log r$, where r is the distance from the point mass source $\mathbf{x}_C = (0.5, 0.35)$, i.e. $r = |\mathbf{x} - \mathbf{x}_C|$, has been applied. As the oblique derivative BC on the bottom boundary, derivative of this exact solution in direction of its gradient, which is equal to $1/r$, has been considered. The differences between the exact and numerical solutions together with the $L_2(\Omega)$ and MAX (Γ) norms for subsequently refined grids can be found in Table 1. One can observe that the $L_2(\Omega)$ and MAX (Γ) norms in case of the upwind scheme are approximately of the first order. We can also observe that the convergence rate in MAX (Γ)-norm of the central scheme significantly decreases with the refinement of the grid.

For the second numerical experiment we have the same computational domain and BC on the upper boundary as in the previous experiment. The direction of the original vector $\vec{s}_1(\mathbf{x})$, i.e. the unit gradient vector of the exact solution, has been modified by an angle α to create a new unit vector $\vec{s}(\mathbf{x})$, see Fig. 3. For this experiment we have chosen $\alpha = 60^{\circ}$. The coordinates of the point mass source have been $\mathbf{x}_C = (0.25, 0.35)$. Then the oblique derivative BC is given by the projection $\nabla T(\mathbf{x})\cdot\vec{s}(\mathbf{x}) = -(1/r)\cos(\alpha)$. As we can see in Table 2, the EOC in case of the $L_2(\Omega)$ and MAX (Γ)-norms for the upwind scheme remains stable reaching values approximately *1*, while in case of the central scheme significantly varies in values. This is a clear consequence of the known fact that central scheme may give an oscillatory solution when applied to the advection equation with general variable velocity field. These two experiments show the restriction of the central scheme of smoothly varying oblique derivative vector $\vec{s}(\mathbf{x})$, while the upwind scheme can be used for generally varying oblique derivative directions.

A similar numerical experiment has been performed in 3D. The computational domain has been a tesseroid bounded by two concentric spheres with radii $R_d = 1$ m and $R_u = 2$ m, and a coaxial cone with dimension $(0, \pi/4) \times (0, \pi/4)$. As the Dirichlet BC (6), the exact solution of (4) in the form $T^{\star} = 1/r$ on the upper and the side boundaries, has been prescribed. Analogously to the previous 2D experiment, the direction of the unit vector $\vec{s}_1(\mathbf{x})$, i.e. the unit gradient vector of the exact solution, has been

Table 1: The $L_2(\Omega)$-norm, *MAX* (Γ)-norm and the EOC for the 2D experiment with the oblique derivative BC computed from the shifted point mass source. * results published in Macák et al. (2012, 2014).

	Upwind scheme				Central scheme*			
$n_1 \times n_2$	$\|T^* - T\|_{L_2(\Omega)}$	EOC	$\|T^* - T\|_{MAX(\Gamma)}$	EOC	$\|T^* - T\|_{L_2(\Omega)}$	EOC	$\|T^* - T\|_{MAX(\Gamma)}$	EOC
8×2	0.043461	-	0.137448	-	0.028261	-	0.071431	-
16×4	0.012002	1.85	0.038109	1.95	0.005400	2.38	0.009351	2.93
32×8	0.004297	1.48	0.014736	1.37	0.001113	2.27	0.002370	1.98
64×16	0.001794	1.26	0.006325	1.26	0.000263	2.08	0.000748	1.66
128×32	0.000816	1.10	0.002929	1.11	0.000064	2.01	0.000260	1.52
256×64	0.000389	1.06	0.001409	1.05	0.000014	2.02	0.000102	1.34

Table 2: The $L_2(\Omega)$-norm, *MAX* (Γ)-norm and the EOC for the 2D experiment when the oblique vector $\vec{s}$ does not have direction of the solution gradient.

	Upwind scheme				Central scheme			
$n_1 \times n_2$	$\|T^* - T\|_{L_2(\Omega)}$	EOC	$\|T^* - T\|_{MAX(\Gamma)}$	EOC	$\|T^* - T\|_{L_2(\Omega)}$	EOC	$\|T^* - T\|_{MAX(\Gamma)}$	EOC
8×2	0.104581	-	0.437204	-	0.319504	-	1.400150	-
16×4	0.043185	1.28	0.198872	1.14	0.016244	4.30	0.120665	3.54
32×8	0.019540	1.14	0.100127	0.99	0.015214	0.09	0.031821	1.92
64×16	0.009096	1.10	0.048672	1.04	0.002248	2.76	0.004576	2.80
128×32	0.004359	1.06	0.023937	1.02	0.019024	-3.08	0.671130	-7.20
256×64	0.002130	1.03	0.011870	1.01	0.000536	5.15	0.010908	5.94

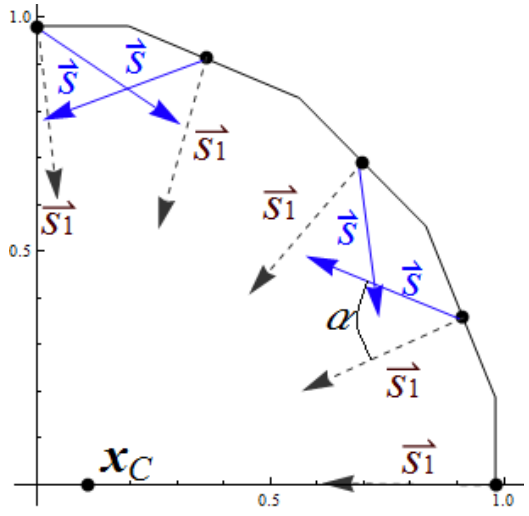

Figure 3: Illustration of creating the vector $\vec{s}$ by rotating of $\vec{s}_1$ by an angle $\pm\alpha$ in 2D on the bottom boundary Γ.

modified by angle $\pm\alpha$ to create a new unit vector $\vec{s}(\mathbf{x})$. For this experiment we have chosen $\alpha = 20°$. The coordinates of the point mass source have been $\mathbf{x}_C = (0.3, -0.2, 0.1)$. Then the oblique derivative BC is given by the projection $\nabla T(\mathbf{x}) \cdot \vec{s}(\mathbf{x}) = -(1/r^2)\cos(\alpha)$. The $L_2(\Omega)$ and *MAX* (Γ) norms of differences between the exact and numerical solutions and the EOC of the methods are shown in Table 3.

We again observe stable behaviour of EOC for the upwind scheme and oscillatory EOC for the central scheme.

4.2 Global gravity field modelling

In this numerical experiment we apply the upwind scheme for global gravity field modelling. We are trying to reconstruct a harmonic function given by the EGM2008 geopotential model up to degree 2160 (Pavlis et al. 2012). It means that all BCs are generated from this model. The Dirichlet BC in the form of the disturbing potential is prescribed on the upper boundary at the constant altitude of 240 km above the reference ellipsoid. The oblique derivative BCs are generated as the first derivative of the disturbing potential in the direction of the normal to the reference ellipsoid. They are generated at points on the real topography that is approximated using the SRTM30 PLUS global topography model (Becker et al., 2009). Our goal is to show a convergence of the FVM solution to EGM2008 when refining the computational grid.

Although the oblique derivative BCs are considered at points on the real topography, in our FVM approach we so far use a structured grid of finite volumes. It means that the computational domain Ω in our computations is bounded by the reference ellipsoid. However, all input data here are adopted from the real topography. This means that $\vec{n}_{pq}$ on

Table 3: The $L_2(\Omega)$-norm, *MAX* (Γ)-norm and the EOC for the 3D experiment with the 3D oblique derivative BC when the oblique vector $\vec{s}$ does not have direction of the solution gradient.

	Upwind scheme				Central scheme			
$n_1 \times n_2 \times n_3$	$\|T^* - T\|_{L_2(\Omega)}$	EOC	$\|T^* - T\|_{MAX(\Gamma)}$	EOC	$\|T^* - T\|_{L_2(\Omega)}$	EOC	$\|T^* - T\|_{MAX(\Gamma)}$	EOC
8×8×4	0.177728	-	0.362022	-	0.061529	-	0.3511	-
16×16×8	0.059441	1.58	0.177806	1.03	0.146351	-1.25	0.209212	0.75
32×32×16	0.022542	1.39	0.083563	1.08	0.058753	1.31	0.050549	2.05
64×64×32	0.010819	1.05	0.041756	1.00	0.008090	2.86	0.053722	2.64
128×128×64	0.005143	1.07	0.019506	1.13	0.004520	0.83	0.024245	0.84

Table 4: Statistics of residuals in $T[\mathrm{m^2 s^{-2}}]$ on the bottom boundary Γ for successive refinemens, and computational details.

	Statistics						Computational aspects		
Resolution	Min.	Max.	Mean	Total	STD Sea	STD Land	Memory Req. [GB]	Procs	CPU/Proc [s]
$40' \times 40'$	-78.910	80.426	-0.392	5.238	4.771	6.228	0.578	16	3.17e2
$20' \times 20'$	-46.584	27.558	-0.273	1.948	1.489	2.750	4.157	32	6.73e3
$10' \times 10'$	-22.011	7.954	-0.265	0.904	0.327	1.578	29.897	64	4.11e4
$5' \times 5'$	-13.926	7.932	-0.114	0.558	0.183	0.991	247.949	128	2.95e5

Table 5: SR: The GPS/leveling test [m] at 61 points in area of Slovakia. * results published in Macák et al. (2014).

		FVM		
			Oblique derivative BC	
	EGM2008	Neumann BC*	Central scheme*	Upwind scheme
Min value	0.301	0.045	0.123	0.131
Mean value	0.437	0.232	0.274	0.279
Max value	0.584	0.393	0.419	0.421
St. deviation	0.043	0.076	0.059	0.058

the bottom boundary is given by the normal to the topography and not by the normal to the ellipsoid. Then the unit vector $\vec{s}(\mathbf{x})$ in Eq. (13) represents the normal to the reference ellipsoid while the direction of $\vec{n}_{pq}$ represents the normal to the Earth's surface and is adopted from our approximation of the topography. In this way we are able to evaluate the coefficients $\vec{s}_{pq}$ in our approximation of the oblique derivative BC (see Eq. (17)).

The computational grid is constructed using the number of divisions in L, B, H directions given by $n_1 \times n_2 \times n_3$:

a) $540 \times 270 \times 75$ (resolution: $40' \times 40' \times 3200$ m),
b) $1080 \times 540 \times 150$ (resolution: $20' \times 20' \times 1600$ m),
c) $2160 \times 1080 \times 300$ (resolution: $10' \times 10' \times 800$ m),
d) $4320 \times 2160 \times 600$ (resolution: $5' \times 5' \times 400$ m).

The obtained FVM solutions are compared with EGM2008. The statistical characteristics of residuals on the bottom boundary as well as computational aspects are summarized in Table 4. One can see that the FVM solution converges to EGM2008 by refining the finite volume grid, i.e. the mean value, STD as well as maximum norm are decreasing. It is worth to note that every refinement of the discretization involves a more detailed consideration of the topography. This does not allow us to compute EOC directly, however, STD as well as the maximum norm in Table 4 indicate that the upwind scheme is the first order accurate.

The residuals between the most refined FVM solution in case d) and EGM2008 are depicted in Fig. 4. The largest residuals are negative and they evidently correlate with high mountainous areas of Himalayas and Andes. The

minimal values of residuals in Table 4 indicate that refinements of the discretization improve the FVM solution also in these zones of complicated topography. This confirms that the presented FVM approach based on the upwind treatment of the oblique derivative BC is able to reconstruct a harmonic function and thus is efficient to solve the oblique derivative BVP.

4.3 Local gravity field modelling

In the last numerical experiment we present the upwind scheme applied for local gravity field modelling in Slovakia. The computational domain Ω has been defined by the ellipsoidal latitude and longitude in range $B \in (47.0^\circ, 55.5^\circ)$ and $L \in (16.0^\circ, 23.0^\circ)$, respectively, with the upper boundary at 240 km above the reference ellipsoid. The number of discretization intervals has been 840 in longitudinal direction, 630 in meridional and 300 in height. As input data on the bottom boundary Γ we used the surface gravity disturbances obtained from the available regular grid $20'' \times 30''$ of gravity anomalies that was compiled from the original gravimetric measurements (Grand et al. 2001). To transform these gravity anomalies into the gravity disturbances we have used the official "digital vertical reference model - DVRM" (www.geoportal.sk). The disturbing potential on upper and side boundaries has been computed from the GOCO03S model up to degree 250 (Mayer-Gürr et al., 2012).

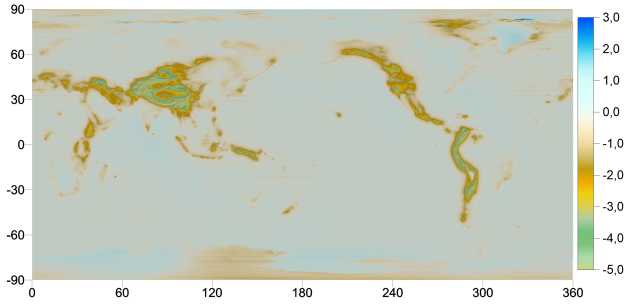

Figure 4: Residuals in $T[\mathrm{m}^2.\mathrm{s}^{-2}]$ between the disturbing potential computed by the FVM solution with upwind treatment of oblique derivative and EGM2008 solution on the bottom boundary Γ.

The computations were performed on the parallel cluster using 32 cores and 8.3 GB of distributed memory. It took about 22 min of the CPU time per processor. The resulting FVM solution obtained by the upwind scheme has been compared with one based on the central scheme. Figure 5 depicts the residuals between both solutions. It is evident that the upwind scheme gives slightly higher undulation towards the highest mountains of Western and High Tatras areas (depicted by dark blue in Fig. 5) where the differences are reaching 0.24 $\mathrm{m}^2\mathrm{s}^{-2}$ ($\approx$ 2.5 cm).

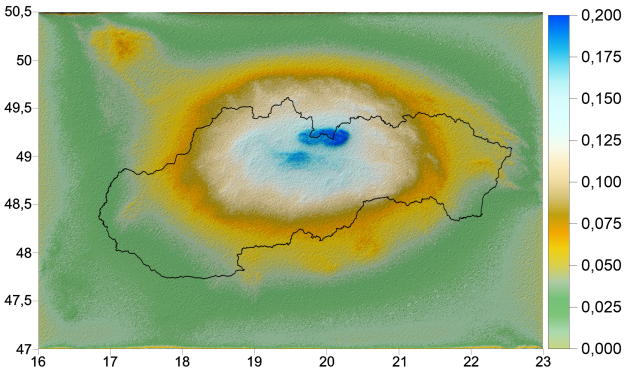

Figure 5: Differences in $T[\mathrm{m}^2.\mathrm{s}^{-2}]$ between the FVM solution with upwind treatment of oblique derivative and FVM solution with central scheme treatment of oblique derivative on the bottom boundary Γ in area of Slovakia.

Finally we present the GNSS-levelling test of the different FVM solutions and EGM2008 (Tab. 5). Although the smallest STD in case of EGM2008 indicates its best accuracy, our treatment of the oblique derivative has evidently improved the FVM solution based on the Neumann BC. Moreover, the upwind scheme has given slightly better results than the central scheme. It is probably due to the fact that the upwind scheme approximates the oblique derivative BC better than the central scheme. This advantage together with the fact that the upwind scheme avoids possible oscillations of the central scheme, make this approach more robust and suitable for solving the oblique derivative BVP.

5 Conclusions

In this paper we have derived an original numerical scheme of FVM based on the approximation of the oblique derivative boundary condition using the upwind principle. We have tested this approach in several 2D and 3D testing experiments. They have showed that the upwind scheme is more robust and stable than the central scheme. The obtained results have indicated that this numerical approach is first order accurate. Its application for global gravity field modelling has demonstrated that the upwind treatment of the oblique derivative boundary conditions is able to reconstruct a harmonic function in case of real topography. In case of local gravity field modelling we have compared the obtained local solution with the one based on the central scheme. This comparison as well as the GNSS-

levelling test have indicated that the upwind scheme approximates the oblique derivative BC better than the central scheme. Our outline for future is to develop a method based on the upwind principle that will be the second order accurate.

Acknowledgement: The work has been supported by the VEGA 1/0714/15 grant and the APVV-0072-11 project.

References

Bauer F.,2004, An alternative approach to the oblique derivative problem in potential theory, PhD thesis, Geomathematics Group, Department of Mathematics, University of Kaiserslautern. Shaker Verlag, Aachen, Germany.

Becker J.J., Sandwell D.T., Smith W.H.F., Braud J., Binder B., Depner J., Fabre D., Factor J., Ingalls S., Kim S.H., Ladner R., Marks K., Nelson S., Pharaoh A., Trimmer R., Von Rosenberg J., Wallace G. and Weatherall P., 2009, Global Bathymetry and Elevation Data at 30 Arc Seconds Resolution: SRTM30 PLUS, Marine Geodesy, 32,4, 355-371.

Bjerhammar A., Svensson L., 1983, On the geodetic boundary value problem for a fixed boundary surface A satellite approach, Bull Geod., 57,1-4, 382-393.

Čunderlík R., Mikula K. and Mojzeš M., 2008, Numerical solution of the linearized fixed gravimetric boundary-value problem, J. Geod., 82, 15-29.

Čunderlík R. and Mikula K., 2010, Direct BEM for high-resolution global gravity field modelling, Stud. Geophys. Geo., 54, 219 - 238.

Čunderlík R., Mikula K.,Špír R., 2012, An oblique derivative in the direct BEM formulation of the fixed gravimetric BVP, IAG Symp., 137, 227 231.

ESA, 1999, Gravity field and steady-state ocean circulation mission, Report for mission selection of the four candidate earth explorer missions, ESA SP-1233(1), ESA Publications Division, ESTEC, Noordwijk, The Netherlands.

Eymard R., Gallouet T. and Herbin R., 2001, Finite volume approximation of elliptic problems and convergence of an approximate gradient, Applied Numerical Mathematics, 37, 1 - 2, 31 - 53.

Fašková Z., 2008, Numerical Methods for Solv- ing Geodetic Boundary Value Problems, PhD Thesis, Department of Mathematics and Descriptive Geometry, Faculty of Civil Engineering, Slovak University of Technology, Bratislava, Slovakia.

Fašková Z., Čunderlík R. and Mikula K., 2010, Finite Element Method for Solving Geodetic Boundary Value Problems, J. Geod., 84, 135-144.

Freeden W., Kersten H., 1981, A constructive approximation theorem for the oblique derivative problem in potential theory, Mathemat. Method. Applied Sci., 3, 104-114,

Grand T., Šefara J., Pășteka R., Bielik M. and Daniel S., 2001l Atlas of geophysical maps and profiles, Part D1: gravimetry, Final report, State geological institute, Bratislava, MS Geofond (in Slovak).

Grothaus M., Raskop T.,2009, The outer oblique boundary problem of potential theory, Numerical Functional Analysis and Optimization, 30, 711-750.

Gutting M., 2007, Fast multipole methods for oblique derivative problems, PhD thesis, Geomathematics Group, Department of Mathematics, University of Kaiserslautern, Shaker Verlag, Aachen, Germany

Gutting M., 2012, Fast multipole accelerated solution of the oblique derivative boundary value problem, International Journal on Geomathematics, 3, 223-252.

Holota P., 1997, Coerciveness of the linear gravimetric boundary-value problem and a geometrical interpretation, J.Geod., 71, 640-651.

Holota P. and Nesvadba O., 2008, Model refinements and numerical solution of weakly formulated boundary-value problems in physical geodesy, In: IAG Symp., 132, Springer, Berlin, 320-326.

Klees R., 1995, Boundary value problems and approximation of integral equations by finite elements, Manuscr. Geodaet., 20, 345-361.

Klees R., 1998, Topics on boundary element methods. Geodetic boundary value problems in view of the one centimeter geoid, Lecture Notes in Earth Sciences, 65, Springer, Heidelberg, 482-531.

Klees R., van Gelderen M., Lage C. and Schwab C., 2001, Fast numerical solution of the linearized Molodensky problem, J. Geod., 75, 349-362.

Koch K.R., Pope A.J., 1972, Uniqueness and existence for the godetic boundary value problem using the known surface of the Earth, Bull Geod., 46, 467-476.

LeVeque R.J., 2002, Finite volume methods for hyperbolic problems, Cambridge Texts in Applied Mathematics, Cambridge University Press.

Lehmann R., 1997, Solving geodetic boundary value problems with parallel computers, Geodetic boundary value problems in view of the one centimeter geoid, Lecture Notes in Earth Sciences, 65, Springer, Berlin, Germany.

Lehmann R. and Klees R., 1999, Numerical solution of geodetic boundary value problems using a global reference field, J. Geod., 73, 543- 554.

Lieberman M.G., 2013, Oblique derivative problems for elliptic equations, World Scientific Publishing Company.

Macák M., Mikula K. and Minarechov'a Z., 2012, Solving the oblique derivative boundary-value problem by the finite volume method, ALGORITMY 2012, 19th Conference on Scientific Computing, Podbanske, Slovakia, Proceedings of contributed papers and posters, Publishing House of Slovak University of Technology, 75- 84.

Macák M., Minarechová Z., Mikula K., 2014, A novel scheme for solving the oblique derivative boundary-value problem, Stud. Geophys. Geo., 58, 4, 556-570.

Mayer-Gürr T., Rieser D., Höck E., Brockmann J..M., Schuh W.-D., Krasbutter I., Kusche J., Maier A., Krauss S., Hausleitner W., Baur O., Jggi A., Meyer U., Prange L., Pail R., Fecher T., Gruber T., 2012, The new combined satellite only model GOCO03s, Abstract submitted to GGHS2012, Venice (Poster).

Meissl P., 1981, The use of finite elements in physical geodesy, Report No. 313, Geodetic Science and Surveying, The Ohio State University, Columbus, USA.

Minarechová Z., Macák M., Čunderlík R., Mikula K., 2015, High-resolution global gravity field modelling by the finite volume method, Stud. Geophys. Geo., 59,1, 1 - 15.

Pavlis N.K., Holmes S.A., Kenyon S.C., and Factor J.K., 2012, The development and evaluation of the Earth Gravitational Model 2008 (EGM2008), J. Geophys. Res., 117, B04406.

Reigber C., Luehr H., and Schwintzer P., 2002, CHAMP mission status, Advances in Space Research, 30, 129-134.

Shaofeng B., Dingbo C., 1991, The finite element method for the geodetic boundary value problem, Manuscr. Geodaet., 16, 353-359.

Tapley B.D., Bettadpur S., Watkins M., and Reigber C., 2004, The gravity recovery and climate experiment: mission overview and early results, Geophysical Research Letters, 31, L09607.